Foramen Lacerum Impingement of Trigeminal nerve root (FLIT) as a rodent model for trigeminal neuralgia

Weihua Ding[1], Liuyue Yang[1], Qian Chen[2], Kun Hu[3], Yan Liu[5], Eric Bao[4], Changning Wang[5], Jianren Mao[1], Shiqian Shen[1*]

Affiliations

[1] Department of Anesthesia, Critical Care and Pain Medicine, Massachusetts General Hospital, Harvard Medical School; Boston MA, USA.

[2] McGovern Institute for Brain Research and Department of Brain and Cognitive Sciences, Massachusetts Institute of Technology, Cambridge MA, USA.

[3]Department of Pathology, Tuft University School of Medicine

[4] Brooks School, North Andover, MA, USA.

[5] Martinos Center for Biomedical Imaging, Department of Radiology, Massachusetts General Hospital, Boston, MA, USA

*Correspondence should be addressed to Shiqian Shen, Room 6224, 149 13th Street, Boston, MA, USA 02129, email: sshen2@mgh.harvard.edu; telephone 617 7264177

The authors have declared that no conflict of interest exists.

Abstract: Trigeminal neuralgia (TN) is a classical neuralgic pain condition with distinct clinical characteristics. Modeling TN in rodents proves challenging. Recently, we found that a foramen in rodent skull base, the foramen lacerum, provides direct access to the trigeminal nerve root. Using this access, we developed FLIT (Foramen Lacerum Impingement of Trigeminal nerve root) model and observed distinct pain-like behaviors in rodents, including paroxysmal asymmetric facial grimaces, head tilt when eating, avoidance of solid chew, lack of wood chewing, etc. The FLIT model recapitulated key clinical features of TN, including lancinating pain-like behavior, and dental pain-like behavior. Importantly, when compared with a trigeminal neuropathic pain model (infraorbital nerve chronic constriction injury, IoN-CCI), the FLIT model was associated with significantly higher numbers of c-Fos positive cells in the primary somatosensory cortex (S1), unraveling robust cortical activation in the FLIT model. Using intravital two-photon calcium imaging, synchronized S1 neural dynamics were only present in the FLIT but not the IoN-CCI model, revealing differential implication of cortical activation in different pain models. Taken together, FLIT is a clinically relevant rodent model of TN which could facilitate pain research and therapeutics development.(187 words)

Introduction

Trigeminal neuralgia (TN) represents one of the most painful conditions to the humanity. As such, it has been called 'the suicide disease' in mass media(1, 2). It is often caused by impingement or demyelination of the trigeminal nerve root, particularly at its entry zone. TN often presents with highly characteristic paroxysmal pain attacks and facial tics, and well-defined trigger zones(3-5). With these unique features, TN is a distinct diagnosis that is different from trigeminal neuropathic pain, which refers to any neuropathic pain in the trigeminal territory(6-8).

Seminal work from Yeomans et al. and Luo et al. used stereotaxic access from the brain and from the infraorbital fissure, respectively, to compress the trigeminal nerve root(9, 10). In both cases, significant mechanical allodynia was observed. Importantly, Yeomans et al. reported rats body shaking when they were eating, which was presumably due to triggered dental pain. This phenomenon was consistent with commonly reported oral trigger zones in TN patients. Inspired by previous work, we sought to develop a clinically relevant rodent model of TN to recapitulate its key clinical features. Recently, we reported the FLIT (Foramen Lacerum Impingement of Trigeminal nerve root) model. (11), Herein, we describe the skull base anatomy underlying the FLIT model, demonstrate the tissue injury associated with the FLIT surgery, optimize surgical technique across different species, and characterize behavioral features of this model. Additionally, we unravel unique cortical activation patterns in TN using this model.

Results

Anatomy of the foramen lacerum

In humans, accessing the trigeminal ganglion through the foramen ovale is routinely used for radiofrequency lesioning to treat TN(12-14). We posited that foramina of the rodent skull base could also be used to access the trigeminal system. For this, we performed anatomical studies in mouse and rat skulls (**Figure 1A**). We found that in both species the foramen lacerum exhibited an elongated yet slightly slanted shape, located in a relatively posterior position of the skull base. In adult C57BL/6 mice, the foramen lacerum was about 1.97±0.05mm (mean ± standard deviation) in length, 0.52±0.06 mm in width; in adult Sprague Dawley rats, it was about 4.04±0.1 mm in length and 1.08 ±0.05 mm in width (Supplementary Table 1).

In humans, skulls base foramina can be accessed by facial and neck/submandibular approaches(12, 15). We performed computed tomography (CT) scan of mice and rats (**Figure 1B**), and found that in both species, foramen lacerum was a prominent skull base foramen. We then used a cervical midline incision

to carefully dissect the muscle and facial layers, and were able to find the foramen lacerum in both species under surgical microscope.

After accessing the foramen lacerum, we sought to examine the neural structure that was immediately accessible through it. We performed microinjection using AAV8-hSyn-eGFP through the foramen lacerum (**Supplementary Figure S1A and B**). One month later, robust virus GFP expression was localized in the trigeminal ganglion and trigeminal projection tract in the brain stem (**Figure 1C)**. The injection site was between trigeminal ganglion and the pons, consistent with the trigeminal nerve root. Additionally, we injected 1% lidocaine through the foramen lacerum. Lidocaine significantly increased facial mechanical withdrawal threshold (**Supplementary figure S1C and D**).

Foramen Lacerum Impingement of Trigeminal nerve root (FLIT) induces trigeminal nerve root demyelination

The trigeminal nerve root and ganglion are covered by dense dura structure. As such, impingement of trigeminal nerve root from a ventral access through the foramen lacerum might lead to sustained localized pressure. To test this, we placed surgifoam through foramen lacerum (**Figure 2A, supplementary figure S2A-C)**. One month post placement, surgifoam-induced local compression was still present **(Supplementary Figure S2D).** To characterize the histological and biochemical consequences of trigeminal nerve root impingement, trigeminal nerve root was stained with hematoxylin and eosin (H&E) and also assessed for its myelination using an antibody against myelin basic protein. FLIT surgery led to significant demyelination in the trigeminal nerve root as well as inflammatory cell infiltration (Figure 2B-D). The significant demyelination associated with the FLIT surgery was evident by both H&E stain and western blot against myelin basic protein (**Figure 2E**). Interestingly, when the FLIT surgery was compared with a traditional surgery to induce trigeminal neuropathic pain – IoN-CCI (infraorbital nerve chronic constriction injury) (16, 17), the latter only induced mild but not statistically significant demyelination in the trigeminal nerve root (**Figure 2B-E**). At the trigeminal ganglion, nociception-related markers including TRPV1 and CGRP were stained using antibodies. The results showed that FLIT model was associated with higher percentages of TRPV1 and CGRP expressing cells in the trigeminal ganglion (**Figure 2F-H**).

FLIT leads to distinct TN-like behavior

A set of distinct behavioral phenotypes were observed (**Figure 3A-F**) **(Supplementary Figure S2E).** As trigeminal nerve root pathologies were implicated in human TN, we wanted to examine if these phenotypes were reminiscent of clinical presentations, and if these phenotypes were different from those observed in the IoN-CCI model.

Adult C57BL/6 mice underwent either IoN-CCI or FLIT procedure, and mechanical withdrawal thresholds in the facial area was determined as demonstrated (**Figure 3A, Video 1**). Both models exhibited significant mechanical allodynia (**Figure 3B**), which lasted longer duration in the FLIT model. Additionally, FLIT model displayed significantly more pronounced nociceptive behavior in response to acetone as a cold stimulation (**Supplementary Figure S3A-C**). The FLIT model displayed significant spontaneous facial grooming (**Figure 3C and D, Video 2**). Importantly, the FLIT model displayed a unique grooming movement pattern: the strokes were primarily asymmetric and wider ipsilateral to the injury side. More strikingly, the FLIT model displayed paroxysmal asymmetrical facial grimacing (**Figure 3E and F, Video 3**), in about 65-80% of animals. These facial grimaces included squinting of the eye on the side of trigeminal injury, intermittent facial twitches or shaking of whiskers. The paroxysmal asymmetrical facial grimacing typically lasted for a few seconds and resolved spontaneously. In humans, trigeminal neuralgia is also called Tic Douloureux, with dramatic bouts of lancinating pain and facial tics(3, 4). The paroxysmal intermittent facial grimacing was only observed in the FLIT model, not in the IoN-CCI model.

Dental pain like-behavior in the FLIT model

Mice in the FLIT group grew their teeth at a faster rate when compared with the IoN-CCI or sham groups (**Figure 4A to C**). For the IoN-CCI and sham groups, the total length of frontal incisors remained relatively unchanged during the experimental observation periods, whereas the FLIT group displayed poor dentition, excessive dental growth to the point that required manual trimming (**Figure 3B**). Of note, due to trimming and occasional teeth fracture secondary to poor dentition, reported data likely underestimated incisors length in the FLIT group.

In the FLIT group, eating and chewing was commonly associated with excessive facial grooming, and in many instances, face patting (**Video 4**). More strikingly, mice in the FLIT group often tilted their head away from the FLIT surgery side (**Figure 4D and supplementary Figure S4A and B**). The head tilt presumably allowed food to be chewed by the contralateral side. This altered eating behavior prompted us to examine if soft chew would be preferred by these mice. To directly assess food preference between solid vs. soft chew, mice were provided with both types of food, eating time for solid vs. soft was quantified. At baseline, before surgeries, animals in all groups spent slightly over 50% of eating time for solid chew, suggesting a slight preference for solid chew. This preference was maintained in both the sham and IoN-CCI groups after surgeries. However, for the FLIT group, mice spent 70 to 80% of eating time for soft chew, consistent with significant preference for soft chew, and avoidance of solid chew (**Figure 4E**). The avoidance of solid chew and observed head tilt during eating were suggestive of dental pain.

To directly assess chewing activities, mice were tested for their chewing of wood blocks. It was found that cork blocks were not associated with consistent chewing, presumably due to chemical glue used during the manufacturing process. On the other hand, oak, maple, or pine blocks were too hard for C57/BL6 mice to chew. Using the Janka Scale of wood hardness, balsa wood block was chosen at it is relatively soft (18). When mice in the FLIT, IoN-CCI and sham groups were individually housed in cages supplied with balsa wood blocks, the wood block weight changes were measured to assess spontaneous chewing. At baseline before surgeries, mice in all groups demonstrated significant chewing as balsa wood blocks were chewed from cube-shape to ball-shape. This chewing ability was maintained in both the sham and IoN-CCI groups after surgeries. However, for the FLIT group, chewing assessed by balsa wood weight changes was significantly decreased (**Figure 4F**).

Moreover, mice in the FLIT model group usually lost their body weight about 10% during the first few days after surgery, followed by slower weight gain when compared with mice in the IoN-CCI or sham groups (**Figure 4G**). As such, inadequate weight gain, head-tilt when eating, avoidance of solid chew, and lack of wood chewing were all consistent with dental pain-like behavior, a common clinical presentation of TN in humans.

We also determined the duration of pain-like behavior in the FLIT model and found that many of the behaviors resolve in about 5-6 weeks (**Supplementary Figure S4C-F**).

Optimizing surgifoam-induced compression in the FLIT model

To refine and optimize the FLIT surgery, different doses of surgifoam were compared in adult C57BL/6 mice. Specifically, 0.5 mg, 1.0 mg, and 1.5 mg of surgifoam were used for FLIT surgery, and all these behavioral endpoints were compared (**Figure 5A-F**). At 0.5 mg dose, surgifoam induced relative mild mechanical allodynia which started to resolve within 2 weeks after surgery (**Figure 5A**). Similarly, this dose only induced mild teeth overgrowth (**Figure 5B**) and a tendency of mild avoidance of solid food (**Figure 5C**), without significant changes in grooming (**Figure 5D**), body weight gain (**Figure 5E**), or wood chewing (**Figure 5F**). On the other hand, both 1 mg and 1.5 mg induced mechanical allodynia (**Figure 5A**), incisors overgrowth (**Figure 5B**), avoidance of solid chew (**Figure 5C**), excessive grooming (**Figure 5D**), inadequate weight gain (Figure **5E**) and lack of wood chewing (**Figure 5F**). There was a modest tendency of more severe pain-like behavior with 1.5 mg than 1.0 mg. The difference between these two groups, however, did not reach statistical significance for the majority of time points tests. Based on these results, 1.0-1.5 mg of surgifoam produced desirable behavioral endpoints for adult C57/BL6 mice.

FLIT model in CD1 mice and in SD rats

The foramen lacerum anatomy appeared to be conserved in different strains of mice and between mice and rats. The FLIT model was tested in CD1 mice and in SD rats. In CD1 mice, mechanical allodynia (**Figure 6A**), increased grooming (**Figure 6B**), paroxysmal asymmetrical grimacing (**Figure 6C**), lack of wood chewing (**Figure 6D and E**) were observed. In SD rats, mechanical allodynia (**Figure 6F**), increased grooming (**Figure 6G**), percentage of rats with facial grimacing (**Figure 6H**), inadequate body weight gain (**Figure 6I**), incisors overgrowth (**Figure 6J**), and lack of wood chewing were observed (**Figure 6K**). These results extended the FLIT model into different strains of mice and different species. However, there were notable behavioral features unique to different animal strains/species. For example, facial grooming tended to be more aggressive in CD1 than C57BL/6 mice, which led to facial skin ulcer in about 30% of mice tested. Wood chewing activities were also more readily observed across different types of wood blocks in SD rats, including pine blocks, balsawood, etc., presumably related to different jaw strength in different species.

Robust activation of the primary somatosensory cortex (S1) in the FLIT model

The cerebral cortex is at the brain's highest hierarchy for information integration, including sensory information(19). The S1 is important for pain processing(20-22). To study the S1 activation in different pain models, mice in the FLIT, IoN-CCI and sham groups were sacrificed 2 hours after surgeries. Brain slices were stained for *c-Fos* expression as a marker for neural activation. The number of *c-Fos* positive cells in the S1 cortex was significantly higher in the FLIT model than the IoN-CCI model (**Figure 7A and B**). To determine the neural activity patterns, the S1 cortex was microinjected with AAV8-CaMKII-GCaMP6f followed by 4 weeks of resting to allow optimal viral expression (**Figure 7C**). GCaMP6f reliably detects single action potentials in neuronal somata and synaptic calcium transients in individual dendritic spines, which makes it a powerful tool in dissecting neuronal activities as well as dynamics of neural circuits over multiple spatial and temporal scales(23-28). Using intravital two-photon calcium imaging in non-anesthetized mice at resting state, contralateral S1 neural population dynamics at single cell resolution were recorded prior to (**Supplementary Figure S5A**) and after surgeries. Mice in the FLIT group displayed synchronized neural activities as previously reported(11), which was absent in the IoN-CCI and sham groups (**Figure 7D**). The S1 neuronal synchronization was confirmed using *VGlut2-Cre* mice and AAV-DIO-hSyn-GCaMP6f (**Supplementary Figure S5B and C**). Besides robust synchronization at resting state, the FLIT model also displayed heightened S1 activity against mechanical stimuli (**Supplementary Figure S5D-F**). Therefore, the upregulation of *c-Fos* was accompanied by unique S1 neuronal activity pattern in the FLIT model.

To examine the S1 neural plasticity, *Thy1-YFP* mice underwent FLIT, IoN-CCI, and sham surgeries. Postsynaptic dendritic spines on apical dendrites of Layer 5 pyramidal neurons of the S1 were observed.

We observed dendritic spine turnover and spine elimination was significantly increased at day 7 post FLIT or IoN-CCI surgery (**Supplementary Figure S6A-C**). Additionally, dendritic spine elimination appeared to be more pronounced in the FLIT model than the IoN-CCI model (**Supplementary Figure S6B**), along with comparable spine formation between the two groups at day 7 after surgeries (**Supplementary Figure S6C**).

Discussion

Encouraged by previous work to recapitulate human TN in animal models(9, 10, 29), we report an anatomy-based approach to take advantage of a natural foramen in the skull base to reliably access the trigeminal nerve root. The procedure, named FLIT, induced behavioral phenotypes that were consistent with key clinical features of TN. For example, facial tics in humans were recapitulated with paroxysmal asymmetrical facial grimacing. Dental pain is a common clinical presentation of trigeminal neuralgia, with many of the patients are misdiagnosed with dental diseases(30, 31). The FLIT model was associated with several unique features, when considered collectively, were likely related to dental pain. For example, inadequate weight gain could be due to other causes. However, when considered in conjunction with lack of wood chewing, and avoidance of solid food, it was likely related to dental pain. Consistent with dental pain-like behavior, head tilting away from the trigeminal injury side was present. The tilt presumably facilitated food to be chewed using teeth on the uninjured side ('no-pain' side). Moreover, teeth overgrowth was also indicative of lack of chewing and/or altered chewing, consistent with dental pain-like behavior. In humans, oral trigger zone is commonly present in TN(3, 4). Due to dental pain-like behavior, we suggest place softened food on cage floor to enhance nutritional support in the FLIT model. Of note, although behavior data reported in this manuscript were based on male mice and rats, similar results were observed in female mice and rats (data not shown).

Clinically, trigeminal ganglion is accessed for radiofrequency lesioning or balloon pump compression through the foramen ovale(3, 32, 33). It is usually accessed using the Hartel's approach from the upper molar level in the face(15, 34). Recently, a submandibular approach to access the foramen ovale was described(12). In rodents, the foramen ovale has not been consistently described(35, 36). In this report, we showed that the foramen lacerum was easily identifiable in rodents. Using CT scan, we found that its relatively caudal location could facilitate an access through a small neck incision. The trigeminal nerve root was directly dorsal to the medial aspect of the foramen lacerum. We reported direct gene delivery to the trigeminal system through the foramen lacerum, establishing a route for gene therapy.

Mechanical allodynia was present in the orofacial area in both the IoN-CCI and FLIT models. While reflex-based evoked pain behaviors have been widely used for pain assessment in research, pain in human often presents as spontaneous pain in 'non-evoked' conditions, in the absence of externally imposed stimuli(37). Recapitulating spontaneous pain-like behavior, without experimentally imposed stimuli, has gained significant research interests(37, 38). For example, facial grimacing scale has been widely accepted as a facial expression coding of pain(39, 40). Notably, the facial grimacing scale, including in the IoN-CCI model, involved bilateral symmetrical facial grimaces(41). In the current study, the facial grimaces were asymmetrical, involving squinting of the eye and facial tics on the ipsilateral side of the injury. The asymmetrical facial grimacing was unlikely due to permanent facial nerve damage, as it was typically paroxysmal and resolved spontaneously, accompanied by facial tics. Trigeminal nerve is a mixed sensory and motor nerve, with the latter innervating masseter muscles. Using botulinum toxin injection to induce unilateral masseter muscle atrophy, we did not observe significant dental pain like behavior or facial mechanical allodynia(11). As such, the behavior phenotypes of the FLIT model were unlikely due to inadvertent motor damage to the trigeminal nerve.

The FLIT model can be applied to both mice and rats, accommodating a range of experimental designs. CD1 mice despite their outbred background have been widely used in neuroscience studies, because they are inexpensive, robust and readily available(42-44). Interestingly, despite largely overlapping behavioral phenotypes across strains/species, there were some noticeable differences. One difference is that CD1 mice displayed self-mutilation due to excessive facial scratching. While severe self-mutilation or autotomy has been reported from rodents to non-human primates after nerve injury(45), strain differences have been described in mice. For example, following sciatic and saphenous nerve injury, Balb/c and C3H strains were more likely to display self-mutilation than C57BL/6 and C57BL/10 strains(46), presumably related to genetic differences.

Many of the behaviors reported in the FLIT model, such as facial grimacing, wood chewing, food preference etc., could be assessed in animals' home cages. Environmental factors, including those associated with behavioral testing, are known to confound pain studies(47, 48). The naturalistic setting of home cage could, in theory, enhance reliability of these assays. More importantly, many of these assays were easily quantifiable, providing objective and quantitative measurements related to pain.

One key feature of the FLIT model was its reversibility. After a decompressive surgery by removing the surgifoam, pain-like behavior in the FLIT model could largely resolve(11). In humans, microvascular decompression is a curative treatment in many cases of TN(3, 49). The resolution of TN-like symptoms after decompression in the FLIT model not only supports the validity of the model, but also suggests an important contribution of peripheral inputs in TN. In line with peripheral inputs, dorsal root ganglion

inputs were found to be instrumental in the synchronization of S1(50). Interestingly, the FLIT model displayed both heightened TRPV1 and CGRP expression in the trigeminal ganglion and enhanced S1 dendritic spine turnover, suggesting a link between peripheral inputs and central neural plasticity.

It is likely that interneuron hypoactivity was underlying the observed cortical synchrony(51). A substantial amount of work has established dense interconnectivity between excitatory and inhibitory neurons in S1 and sensory cortices in general(52-56). Furthermore, a link between inhibitory neuron hypoactivity and excitatory neuron hyperactivity has been demonstrated(57, 58). However, the specific mechanisms through which interneuron hypoactivity lead to excitatory neuron hypersynchronization are poorly understood. This synchronization mimics focal seizure activity. Carbamazepine, an anti-seizure drug and a first-line medication for TN, attenuated TN-like behavior and cortical synchronization in the FLIT model(51). Besides central mechanisms, it is likely that peripheral inputs are also implicated as shown by references(50) (51).

Trigeminal neuropathic pain has been successfully modeled using the IoN-CCI model(16, 17), whereas modeling TN proved challenging in rodents(59). By impinging the trigeminal nerve root through the foramen lacerum, the FLIT model captures characteristic clinical features of TN. Using the FLIT model, we discovered robust cortical S1 activation and neural dynamics that were different from the IoN-CCI model, unraveling unique neural dynamics of TN. As such, the FLIT model provides an additional tool for disease-specific mechanistic studies and testing of analgesics.

Methods

Animal

4 to 5 month-old male and female C57/BL6, *Thy1-YFP* line (Strain 003782) and *VGlut2-Cre* mice (Strain 028863) were purchased from the Jackson Laboratory (ME). Mice were housed in temperature-controlled vivarium on a 12 h light/dark cycle (lights on at 07:00 am, lights off at 07:00 pm) with food and water available *ad libitum*. CD1 mice (16-26 weeks old, male) and SD rats (10 to 14 weeks old, male) were also purchased from the Jackson Laboratory (ME) and Charles River Laboratories (MA), respectively.

CT scan

Rodents were anesthetized with isoflurane inhalation and placed in prone position with neck extended in Triump rodent X-O scan (GE Healthcare, CT). Sagittal (D), coronal (E) and oblique (F) views were shown using PMOD software (PMOD Technologies, LLC) reconstruction of CT images.

Foramen lacerum impingement of trigeminal-nerve root (FLIT) procedure

Mice were anesthetized with isoflurane inhalation (3% for induction and 1.5 to 2% for maintenance) in oxygen (flow rate: 1 to 2 L/min). The Surgery was performed under an Omano surgical microscope (OM2300S-V7) at 7-45X magnification. After surgical field preparation, a 1 - 1.5 cm midline neck incision was made starting at the rostral end of the sternum using a sterile spring scissor. The superficial tissues such as salivary glands were bluntly dissected and lateralized with a mini retractor. The neck muscles, including sternocleidomastoid muscle, digastric muscle, strap muscles were gently dissected to locate right auditory bulla and auditory capsule on the right side of the mouse head which are the landmarks to locate the foramen lacerum. Electric cauterization was applied to control minor bleeding from capillaries. Care was taken while dissecting the vessels covering both the anterior bulla and the foramen of lacerum. A prepared piece of surgifoam (Ethicon, Inc., Somerville, USA) at ~1-1.5 mg (mice) or ~2.5 mg (rats) was gently delivered into the foramen lacerum using curved forceps. The surgifoam was positioned between trigeminal nerve root and the cochlea bulla. After removing the retractor and replacing the tissues, the skin was closed with 4-0 nylon monofilament (Ethicon, Inc., Somerville, USA) sutures. Animals in sham group underwent the same surgical procedure including neck shaving, skin incision, muscles dissection and foramen lacerum exposure without physical trigeminal nerve root compression. The surgery time ranged from 8-12 minutes per animal. A representative video demonstrating FLIT surgery was included (**Video 5**).

Infraorbital nerve chronic constriction injury (IoN-CCI)

IoN-CCI procedure was performed as previously described(17) with minor modifications. Briefly, mice were anesthetized with isoflurane inhalation (3% for induction and 1.5 to 2% for maintenance) in oxygen (flow rate: 1 to 2 L/min). The skin between the eye and facial whiskers was prepared. A 0.5 cm incision parallel to the mid-line was made from the caudal end of the third-forth row of facial whickers to the ipsilateral inner canthus. The immediately exposed superficial tissues were bluntly dissected and lateralized using a mini retractor. When the trunk of infraorbital nerve was exposed outside of the inferior orbital fissure, two chromic gut ligatures (6 - 0) were loosely placed around the distal segment of infraorbital nerve with 2 mm apart.

Mechanical withdrawal threshold

Animals were individually placed in a custom-made testing enclosure allowing for free head movement. After 30 minutes of acclimation, a graded series of von Frey filaments were inserted through the mesh walls from the lateral side and applied to the skin of the vibrissa pad within the trigeminal nerve V2 branch-innervated territory for 1 second at 10 seconds intervals. A brisk withdraw of the head upon stimulation was considered a positive response. Animals were tested 5 times with at least 3 positive responses indicated a positive result. The minimum force necessary to elicit a response was defined as the mechanical withdrawal threshold.

Observation of face grooming and grimacing

For facial grooming and grimacing test, each animal was habituated 30 min daily for up to 3 consecutive days in a Plexiglass box equipped with a mirror to record unobstructed views of the orofacial area. The mice behaviors were recorded for 10 minutes without any extra audio or physical disturbance. Grooming was defined as face wash strokes primarily directed to the trigeminal nerve impingement side. Facial grimacing for this study was defined as asymmetrical eyelid contraction that ipsilateral eye (same side as trigeminal nerve compression) opening was smaller than contralateral side as determined by blinded observers. The recorded behaviors were analyzed by an experimenter who was blinded to the procedures condition/group assignment of the mice.

Food preference

Animals were deprived of food 12 hours prior to the test, with water accessible *ad libitum*. To prepare the soft chow, regular solid chow was soaked in water (pellets : water = 1: 2) for 20 minutes. Regular solid chow and freshly prepared soft chow were placed in plates. Test mouse was videotaped using a camera 40cm above the cage for 10 minutes. Time spent eating solid and soft chow in each video was quantified by experimenters that were blinded to group assignment.

Wood chewing assay

Balsa wood blocks were customized to 1 inch cube. Mice were housed in individual cages with food and water supplied *ad libitum*, a balsa wood block was placed in the cage for 24 hours. Weight of blocks before and after placement was weighed. For rats, pine wood blocks were customized to 1.5 inch cube. Two rats were cohoused in a cage with food and water supplied ad libitum, a wood block was placed in the cage for 7 days. Weight of blocks before and after placement was weighed.

Acetone test

Mice were placed in acrylic glass enclosures on an elevated metal mesh and allowed to acclimate the testing room 30 minutes daily for 3 days before testing. After mice calm down, using a micropipette, 20 µl of acetone (Fisher Scientific) was applied to the lower jaw or whisker pad ipsilateral to trigeminal nerve injuries side. The animal exhibited multiple responses to the acetone application. We define the test as 'Acetone score' and a score of 0 indicated no response; 0.5 indicated brushing; 1 indicated grimacing or flinching, 2 indicated brushing and grimacing, 3 indicated flinching and brushing or flinching and grimacing; 4 indicated flinching, brushing and grimacing. Behavior was observed during the first 60 seconds after acetone application and measurements were repeated 2 times with a 10-minute interval to obtain a mean value. We tested all animals in V2 and V3 branch of trigeminal nerve innervated areas respectively, and spared V1 branch due to eye irritation and animal welfare.

Craniotomy and Virus injection

Cranial windows were implanted on the contralateral side to the FLIT, IoN-CCI or Sham procedure. Mice were anesthetized with isoflurane (3% for induction and 1.5% for maintenance in oxygen). The eyes were moistened with eye lubricant. To minimize post-op pain, ketorolac tromethamine (Althenex, Schaumburg, IL USA) was administrated (5 mg/kg) intraperitoneally every 12 hours for 3 consecutive days. The fur on the top of head was shaved between outer canthus and concha, then the mouse was positioned in a stereotactic frame with a head holder. The skin was prepared with Povidone-Iodine solution (Aplicare, INC., Neriden, CT USA) followed by 70% alcohol swab (BD, Franklin Lakes, USA). After Lidocaine (0.2 ml, 1%) infiltration, a skin flap overlying the dorsal skull was removed using micro scissors. Connective tissues and periosteum of the parietal skull was thoroughly cleaned. A 3×3 mm piece of bone was removed to reveal the left anterolateral cortex including the primary somatosensory cortex as determined by stereotactic coordinates following Chen *et al.* (60) and the dura was kept moist with sterile saline.

For GCaMP6f expression in pyramidal neurons, adeno-associated virus AAV8 carrying CaMKII-GCaMP6f (pENN.AAV.CamKII.GCaMP6f.WPRE.SV40. Addgene. #100834. 1×10^{12} genome copies per ml) was injected with Nanoject-III (Drummond Scientific Company, model #3-000-207) at a depth of 200 μm beneath pia surface and virus was slowly injected at 4-5 sites ~1 to 4 mm lateral to midline of skull, and bregma ~1 to -2 mm in WT mice. For GCaMP6f expression in Vglut2-Cre mouse, AAV8-EF1a-DIO-GCaMP6f (a kind gift from Guoping Feng lab, MIT, Cambridge) was injected into contralateral side of S1 cortex of Vglut2-Cre mice. For *Thy1-YFP* mice, glass window was implanted instantly after craniotomy.

Two-photon imaging

Prior to imaging session, mice were taken to the two-photon microscope room using a head fixation device for 30 min daily, for more than three sessions for habituation. In vivo two-photon imaging was performed with a two-photon system (Ultima; Bruker) equipped with a Mai tai laser (Spectra Physics, KMC 100). The laser was tuned to 910 nm and the average laser power through the transcranial window was ~20-30 mW for imaging acquisition using a 20X, 1.0 NA water-immersion objective (Olympus, Japan). All images were acquired at frame rate of 6-12 Hz using Prairie View Software in awake status without anesthesia. Of note, for any given animal, the field of view was kept constant, to obtain images on the same group of neurons longitudinally. For dendritic spine imaging, baseline was acquired before surgery and repeated imaging was acquired at day 7 after surgery. All dendrite views were imaged with Z stacks. Quantification of dendritic spines were adopted from Yang *et al*. (61).

Calcium imaging data analysis

Imaging data was corrected for motion between frames using the NoRMCorre software package (62). Neuron selection was carried out subsequently using custom written software in Matlab (Mathworks). Calcium fluorescence signals of each individual neuron were extracted from the corrected video files. The signal for each neuron was corrected for background fluorescence changes by subtracting the fluorescence changes from the immediate surrounding. Each neuron's activity time course was then quantified using the formula $\Delta F = (F - F0) / F0$ where F is the fluorescence signal at a given frame and F0 was calculated from a sliding window of +/- 30 seconds around the frame. Finally, baseline correction was carried out by fitting a linear function (Matlab function robustfit) to the lowpass filtered (cutoff: 0.3 Hz) signal. A deconvolution algorithm (Fast online deconvolution of calcium imaging data) was applied to detect transients (63). The start and end of transients were detected when the model was above 0.1. For responsive neurons in mechanical stimulation test, an increase of neuronal activity by at least 25% from own baseline within 10 seconds from stimulation were used as cutoffs.

Hematoxylin and Eosin (H&E) staining

Frozen trigeminal ganglion tissues were sliced (5μm) and mounted to slides to visualize ganglion and trigeminal nerve structures. Briefly, slides were incubated in Harris' Hematoxylin for 5 min, and rinsed in H20 for 5 min and differentiated in acid alcohol (1% HCl in 70% ethanol) for 10 sec. Next, sections were rinsed with distilled H20 (dH20) for 5 min and incubated in ammonia water (0.25% ammonia hydroxide in dH20) for 3-5 min and rinsed with dH20 2X's (5 min). Sections were dipped in alcoholic Eosin for 10 sec, rinsed with dH20 2X's (5min), dehydrated in ethanol and then mounted onto coverslips.

Immunofluorescence staining

C-Fos staining: Mice underwent surgeries (Sham, IoN-CCI and FLIT) were briefly maintained under isoflurane anesthesia and procedures were performed after lidocaine 1% infiltration of incision sites. Two hours after surgery, mice were sacrificed and perfused with ice-cold PBS followed by 4% paraformaldehyde in 0.1 M phosphate buffer (4% PFA). Brain samples were fixed in 4% PFA at 4°C for 24 hours. Coronal brain sections were sliced at 60μm thickness using a Leica vibratome (VT 1000s). Tangential slices covering the primary somatosensory cortex was used for *c-Fos* staining. Slices were washed in PBS 5 min for 3 times, followed by blocking with 6% goat serum and 2% bovine serum albumin (BSA) in PBS with 0.3% Triton X-100 (Blocking solution) at room temperature for 1 h. Floating slices were stained with primary antibody (rabbit anti-c-Fos, CellSignaling, CatLog 2250, 1:500 dilution) in blocking solution at 4°C for overnight. After washing with PBS 5 minutes for 3 times, slices were incubated with secondary antibody (goat anti-rabbit Alexa488, Jackson ImmunoResearch, CatLog 111-545-144). Images were acquired with Nikon A1 confocal microscope equipped with 20x and 4x objectives. The acquired images were analyzed using ImageJ (NIH opensource software). Number of positive cells were counted by an experimenter who was blinded to group assignment. For each group, 4 animals were used. Number of *c-Fos* positive cells were counted within the slices covering the primary somatosensory cortex individually.

CGRP, TRPV1, and NeuN staining: Brain slices were frozen sectioned at 5 μm thickness and incubated with primary antibodies at 4°C overnight, followed by secondary antibodies incubation at room temperature for 1 hour. Images were acquired using a Nikon AXR confocal microscope. Guinea pig anti-TRPV1 (Invitrogen, Catlog PA129770, 1:1000 dilution); rabbit anti-CGRP (Immunostar, Catlog 24112, 1:500); Donkey anti-mouse NeuN (Cell Signaling Technologies, Catlog 94403, 1:500 dilution); Goat anti-rabbit Cy3 (Jackson ImmunoResearch, Catlog 111-165-003, 1:2000 dilution); Goat anti-mouse

DyLight 405 (Jackson ImmunoResearch, Catlog 115-475-003, 1:250 dilution); and Goat anti-guinea pig Cy3 (Jackson ImmunoResearch, Catlog 106-165-003, 1:2000 dilution).

Western blot

Mice subject to sham, IoN-CCI and FLIT surgery were sacrificed and trigeminal ganglions were collected at day 14. Proteins were extracted from tissues and the total protein concentration between samples was equalized. 30 μg protein of each sample was loaded and separated by a sodium dodecylsulfate (SDS)–polyacrylamide gel electrophoresis (PAGE) and then transferred to a poly (vinylidene fluoride) membrane (BioRad). The primary antibodies of anti-MBP (Cell signaling technology, Catlog 83683, 1:1000) or ß-actin (AbCam, catlog 8226, 1:5000) was incubated in blocking buffer at 4^0C overnight. Second antibodies (Jackson Immunoresearch, Catlog 115-035-003, 1:5000) were incubated for one hour at room temperature. Images were acquired using a ChemiDoc MP (BioRad, California).

Statistics

Data were expressed as mean ± the standard error of the mean (SEM) for Figures 3, 4, 5, 6, 7 and Supplementary Figures 1, 4C-F, mean ± standard deviation (SD) for Figure 2 and Supplementary Figures 3, 4A-B, 5E. The difference in pain behaviors was analyzed using a repeated-measures two-way analysis of variance (ANOVA). Post-hoc comparisons with Bonferroni corrections were used for comparison across groups at indicated time points. Percentages of mice with facial grimacing were compared across groups using two-sided Fisher's exact test. One-way ANOVA followed by Tukey post-hoc comparison was used for comparison of three groups. Two-tailed unpaired t-tests were used for two-group comparisons. P of < 0.05 was considered statistically significant. Statistical analysis was carried out using GraphPad Prism software (version 8.0).

Study approval

All animal use and procedures applied according to protocols approved by the Massachusetts General Hospital Institutional Animal Care and Use Committee (IACUC). Experiments performed were complying with the guidelines established by NIH and the International Association for the Study of Pain.

Data availability

All original behavioral and imaging data are available upon request. Two-photon imaging analyses code can be accessed at https://github.com/harnett/Shiqian-analysis.

Author contributions

Conceptualization: W.D.; S.S.; Methodology: W.D.; L.Y.; Q.C.; K.H., C.W., J.M., S.S.; Investigation: W.D.; L.Y.; K.H., E.B., Y.L., Formal analysis, data curation: W.D.; L.Y.; K.H.; Y.L.; Writing: Original draft: W.D., S.S.. Funding acquisition: S.S..

Acknowledgements

This work was supported by NIH NS116423, NIH AG067947, and NIH NS126029. Shiqian Shen lab also received support from NIH R35 GM128692, AG 065606 and RF1AG070141. Weihua Ding received support from the Borsook Project Fellowship. The authors thank MGH CNY 149 animal facility for animal husbandry; Scot Mackeil at Biomedical Engineering Department for equipment maintenance; Department of Anesthesia, Critical Care and Pain Medicine of MGH for generous support. The authors thank Drs. Ping Jin, Yong Luo, Sarah Low at the Department of Anesthesia, Critical Care and Pain Medicine of MGH for critical discussion, Dr. Tong Zhu from St. Louis for valuable critiques.

References

1. Adams H, Pendleton C, Latimer K, Cohen-Gadol AA, Carson BS, and Quinones-Hinojosa A. Harvey Cushing's case series of trigeminal neuralgia at the Johns Hopkins Hospital: a surgeon's quest to advance the treatment of the 'suicide disease'. *Acta Neurochir (Wien).* 2011;153(5):1043-50.
2. Mansano AM, Frederico TN, Valentin REB, Carmona MJC, and Ashmawi HA. Percutaneous Radiofrequency Ablation for Trigeminal Neuralgia Management: A Randomized, Double-blind, Sham-Controlled Clinical Trial. *Pain Med.* 2022.
3. Cruccu G, Di Stefano G, and Truini A. Trigeminal Neuralgia. *The New England journal of medicine.* 2020;383(8):754-62.
4. Cruccu G, Finnerup NB, Jensen TS, Scholz J, Sindou M, Svensson P, et al. Trigeminal neuralgia: New classification and diagnostic grading for practice and research. *Neurology.* 2016;87(2):220-8.
5. Shankar Kikkeri N, and Nagalli S. *StatPearls*. Treasure Island (FL); 2020.
6. Scholz J, Finnerup NB, Attal N, Aziz Q, Baron R, Bennett MI, et al. The IASP classification of chronic pain for ICD-11: chronic neuropathic pain. *Pain.* 2019;160(1):53-9.
7. Baad-Hansen L, and Benoliel R. Neuropathic orofacial pain: Facts and fiction. *Cephalalgia : an international journal of headache.* 2017;37(7):670-9.
8. Melek LN, Smith JG, Karamat A, and Renton T. Comparison of the Neuropathic Pain Symptoms and Psychosocial Impacts of Trigeminal Neuralgia and Painful Posttraumatic Trigeminal Neuropathy. *J Oral Facial Pain Headache.* 2019;33(1):77-88.
9. Yeomans DC, and Klukinov M. A rodent model of trigeminal neuralgia. *Methods Mol Biol.* 2012;851:121-31.
10. Luo DS, Zhang T, Zuo CX, Zuo ZF, Li H, Wu SX, et al. An animal model for trigeminal neuralgia by compression of the trigeminal nerve root. *Pain Physician.* 2012;15(2):187-96.
11. Ding W, Fischer L, Chen Q, Li Z, Yang L, You Z, et al. Highly synchronized cortical circuit dynamics mediate spontaneous pain. *bioRxiv.* 2022:2022.10.04.510722.

12. Ding W, Chen S, Wang R, Cai J, Cheng Y, Yu L, et al. Percutaneous radiofrequency thermocoagulation for trigeminal neuralgia using neuronavigation-guided puncture from a mandibular angle. *Medicine (Baltimore).* 2016;95(40):e4940.
13. Kantola VE, McGarry GW, and Rea PM. Endonasal, transmaxillary, transpterygoid approach to the foramen ovale: radio-anatomical study of surgical feasibility. *J Laryngol Otol.* 2013;127(11):1093-102.
14. Khairnar KB, and Bhusari PA. An anatomical study on the foramen ovale and the foramen spinosum. *J Clin Diagn Res.* 2013;7(3):427-9.
15. Penman J. A simple radiological aid to gasserian injection. *Lancet.* 1949;2(6572):268-74.
16. Deseure K, and Hans GH. Chronic Constriction Injury of the Rat's Infraorbital Nerve (IoN-CCI) to Study Trigeminal Neuropathic Pain. *J Vis Exp.* 2015(103).
17. Ding W, You Z, Shen S, Yang J, Lim G, Doheny JT, et al. An Improved Rodent Model of Trigeminal Neuropathic Pain by Unilateral Chronic Constriction Injury of Distal Infraorbital Nerve. *J Pain.* 2017;18(8):899-907.
18. Wiepking CA, Doule, D.V. Strength and related properties of balsa and quipo woods.

Report (Forest Products Laboratory (US)). 1955;1511:1-9.
19. Singer W. Recurrent dynamics in the cerebral cortex: Integration of sensory evidence with stored knowledge. *Proc Natl Acad Sci U S A.* 2021;118(33).
20. Kunz M, Chen JI, and Rainville P. Keeping an eye on pain expression in primary somatosensory cortex. *Neuroimage.* 2020;217:116885.
21. Moulton EA, Pendse G, Morris S, Aiello-Lammens M, Becerra L, and Borsook D. Segmentally arranged somatotopy within the face representation of human primary somatosensory cortex. *Hum Brain Mapp.* 2009;30(3):757-65.
22. Okada T, Kato D, Nomura Y, Obata N, Quan X, Morinaga A, et al. Pain induces stable, active microcircuits in the somatosensory cortex that provide a therapeutic target. *Sci Adv.* 2021;7(12).
23. Garg AK, Li P, Rashid MS, and Callaway EM. Color and orientation are jointly coded and spatially organized in primate primary visual cortex. *Science.* 2019;364(6447):1275-9.
24. Gottschalk S, Degtyaruk O, Mc Larney B, Rebling J, Hutter MA, Dean-Ben XL, et al. Rapid volumetric optoacoustic imaging of neural dynamics across the mouse brain. *Nature biomedical engineering.* 2019;3(5):392-401.
25. Scott BB, Thiberge SY, Guo C, Tervo DGR, Brody CD, Karpova AY, et al. Imaging Cortical Dynamics in GCaMP Transgenic Rats with a Head-Mounted Widefield Macroscope. *Neuron.* 2018;100(5):1045-58 e5.
26. Rungta RL, Chaigneau E, Osmanski BF, and Charpak S. Vascular Compartmentalization of Functional Hyperemia from the Synapse to the Pia. *Neuron.* 2018;99(2):362-75 e4.
27. Hinckley CA, Alaynick WA, Gallarda BW, Hayashi M, Hilde KL, Driscoll SP, et al. Spinal Locomotor Circuits Develop Using Hierarchical Rules Based on Motorneuron Position and Identity. *Neuron.* 2015;87(5):1008-21.
28. Dana H, Chen TW, Hu A, Shields BC, Guo C, Looger LL, et al. Thy1-GCaMP6 transgenic mice for neuronal population imaging in vivo. *PloS one.* 2014;9(9):e108697.
29. Ahn DK, Lim EJ, Kim BC, Yang GY, Lee MK, Ju JS, et al. Compression of the trigeminal ganglion produces prolonged nociceptive behavior in rats. *European journal of pain.* 2009;13(6):568-75.
30. Truelove E. Management issues of neuropathic trigeminal pain from a dental perspective. *Journal of orofacial pain.* 2004;18(4):374-80.
31. Renton T. Dental (Odontogenic) Pain. *Reviews in pain.* 2011;5(1):2-7.
32. Barlas O, and Unal TC. A technique to facilitate the cannulation of the foramen ovale for balloon compression. *Br J Neurosurg.* 2021:1-4.

33. Alshukry A, Salburgo F, Jaloux L, Lavieille JP, and Montava M. Trigeminal neuralgia (TN): A descriptive literature analysis on the diagnosis and management modalities. *Journal of stomatology, oral and maxillofacial surgery.* 2017;118(4):251-4.
34. Iwanaga J, Badaloni F, Laws T, Oskouian RJ, and Tubbs RS. Anatomic Study of Extracranial Needle Trajectory Using Hartel Technique for Percutaneous Treatment of Trigeminal Neuralgia. *World Neurosurg.* 2018;110:e245-e8.
35. Santaolalla-Montoya F, Martinez-Ibarguen A, Sanchez-Fernandez JM, and Sanchez-del-Rey A. Principles of cranial base ossification in humans and rats. *Acta Otolaryngol.* 2012;132(4):349-54.
36. Hill EJ. The cranial foramina in rodents. *Journal of Mammalogy.* 1935;16(2):121-9.
37. Yezierski RP, and Hansson P. Inflammatory and Neuropathic Pain From Bench to Bedside: What Went Wrong? *The journal of pain : official journal of the American Pain Society.* 2018;19(6):571-88.
38. Zheng Q, Xie W, Luckemeyer DD, Lay M, Wang XW, Dong X, et al. Synchronized cluster firing, a distinct form of sensory neuron activation, drives spontaneous pain. *Neuron.* 2021.
39. Langford DJ, Bailey AL, Chanda ML, Clarke SE, Drummond TE, Echols S, et al. Coding of facial expressions of pain in the laboratory mouse. *Nature methods.* 2010;7(6):447-9.
40. Mogil JS, Pang DSJ, Silva Dutra GG, and Chambers CT. The development and use of facial grimace scales for pain measurement in animals. *Neuroscience and biobehavioral reviews.* 2020;116:480-93.
41. Akintola T, Raver C, Studlack P, Uddin O, Masri R, and Keller A. The grimace scale reliably assesses chronic pain in a rodent model of trigeminal neuropathic pain. *Neurobiology of pain.* 2017;2:13-7.
42. Aldinger KA, Sokoloff G, Rosenberg DM, Palmer AA, and Millen KJ. Genetic variation and population substructure in outbred CD-1 mice: implications for genome-wide association studies. *PloS one.* 2009;4(3):e4729.
43. Bon K, Lichtensteiger CA, Wilson SG, and Mogil J. Characterization of cyclophosphamide cystitis, a model of visceral and referred pain, in the mouse: species and strain differences. *J Urol.* 2003;170(3):1008-12.
44. Gonzalez-Sepulveda M, Pozo OJ, Marcos J, and Valverde O. Chronic pain causes a persistent anxiety state leading to increased ethanol intake in CD1 mice. *J Psychopharmacol.* 2016;30(2):188-203.
45. Colleoni M, and Sacerdote P. Murine models of human neuropathic pain. *Biochim Biophys Acta.* 2010;1802(10):924-33.
46. Rubinstein RE, Deem KC, Jensen J, MacKinnon SE, and Tung TH. Strain differences in autotomy in mice after peripheral nerve transection or repair. *Microsurgery.* 2003;23(4):363-8.
47. Jain M, and Baldwin AL. Are laboratory animals stressed by their housing environment and are investigators aware that this stress can affect physiological data? *Med Hypotheses.* 2003;60(2):284-9.
48. Mogil JS. Laboratory environmental factors and pain behavior: the relevance of unknown unknowns to reproducibility and translation. *Lab Anim (NY).* 2017;46(4):136-41.
49. Barker FG, 2nd, Jannetta PJ, Bissonette DJ, Larkins MV, and Jho HD. The long-term outcome of microvascular decompression for trigeminal neuralgia. *N Engl J Med.* 1996;334(17):1077-83.
50. Chen C, Sun L, Adler A, Zhou H, Zhang L, Zhang L, et al. Synchronized activity of sensory neurons initiates cortical synchrony in a model of neuropathic pain. *Nat Commun.* 2023;14(1):689.
51. Ding W, Fischer L, Chen Q, Li Z, Yang L, You Z, et al. Highly synchronized cortical circuit dynamics mediate spontaneous pain in mice. *J Clin Invest.* 2023;133(5).
52. Fino E, and Yuste R. Dense inhibitory connectivity in neocortex. *Neuron.* 2011;69(6):1188-203.

53. Harris KD, and Mrsic-Flogel TD. Cortical connectivity and sensory coding. *Nature.* 2013;503(7474):51-8.
54. Katzel D, Zemelman BV, Buetfering C, Wolfel M, and Miesenbock G. The columnar and laminar organization of inhibitory connections to neocortical excitatory cells. *Nat Neurosci.* 2011;14(1):100-7.
55. Packer AM, and Yuste R. Dense, unspecific connectivity of neocortical parvalbumin-positive interneurons: a canonical microcircuit for inhibition? *J Neurosci.* 2011;31(37):13260-71.
56. Petersen CCH. Sensorimotor processing in the rodent barrel cortex. *Nat Rev Neurosci.* 2019;20(9):533-46.
57. Cichon J, Blanck TJJ, Gan WB, and Yang G. Activation of cortical somatostatin interneurons prevents the development of neuropathic pain. *Nat Neurosci.* 2017;20(8):1122-32.
58. Eto K, Ishibashi H, Yoshimura T, Watanabe M, Miyamoto A, Ikenaka K, et al. Enhanced GABAergic activity in the mouse primary somatosensory cortex is insufficient to alleviate chronic pain behavior with reduced expression of neuronal potassium-chloride cotransporter. *J Neurosci.* 2012;32(47):16552-9.
59. Fried K, and Hansson PT. Animal models of trigeminal neuralgia: A commentary. *Molecular pain.* 2020;16:1744806920980538.
60. Chen Q, Deister CA, Gao X, Guo B, Lynn-Jones T, Chen N, et al. Dysfunction of cortical GABAergic neurons leads to sensory hyper-reactivity in a Shank3 mouse model of ASD. *Nat Neurosci.* 2020;23(4):520-32.
61. Yang G, Pan F, and Gan WB. Stably maintained dendritic spines are associated with lifelong memories. *Nature.* 2009;462(7275):920-4.
62. Pnevmatikakis EA, and Giovannucci A. NoRMCorre: An online algorithm for piecewise rigid motion correction of calcium imaging data. *J Neurosci Methods.* 2017;291:83-94.
63. Friedrich J, Zhou P, and Paninski L. Fast online deconvolution of calcium imaging data. *PLoS Comput Biol.* 2017;13(3):e1005423.

Figures and Legends

Figure 1

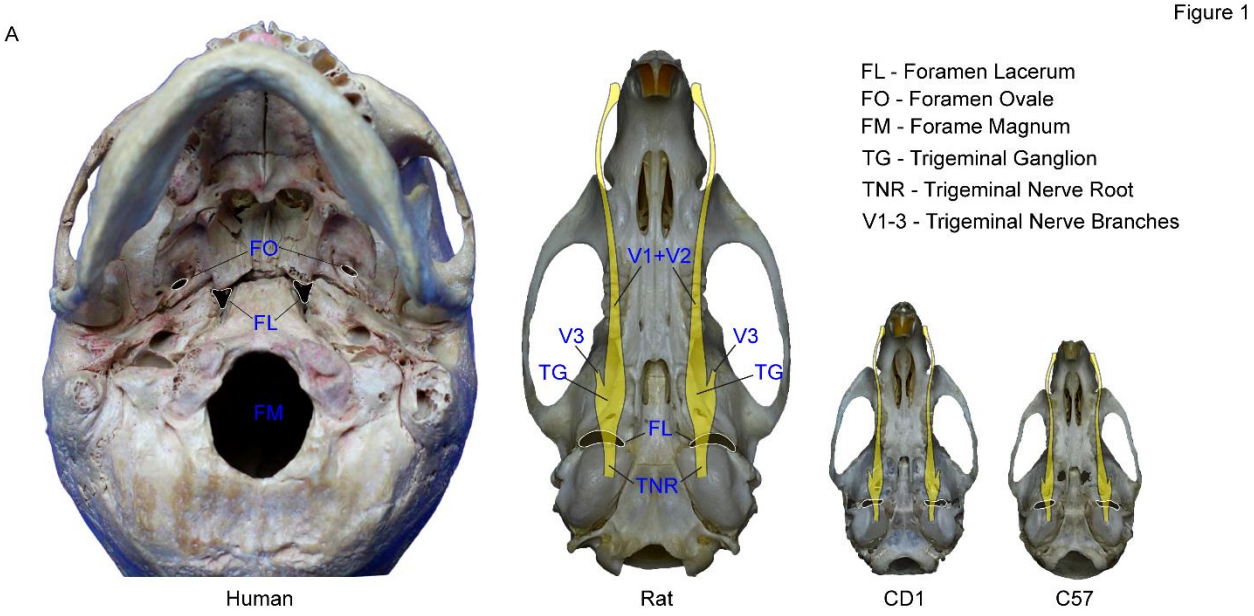

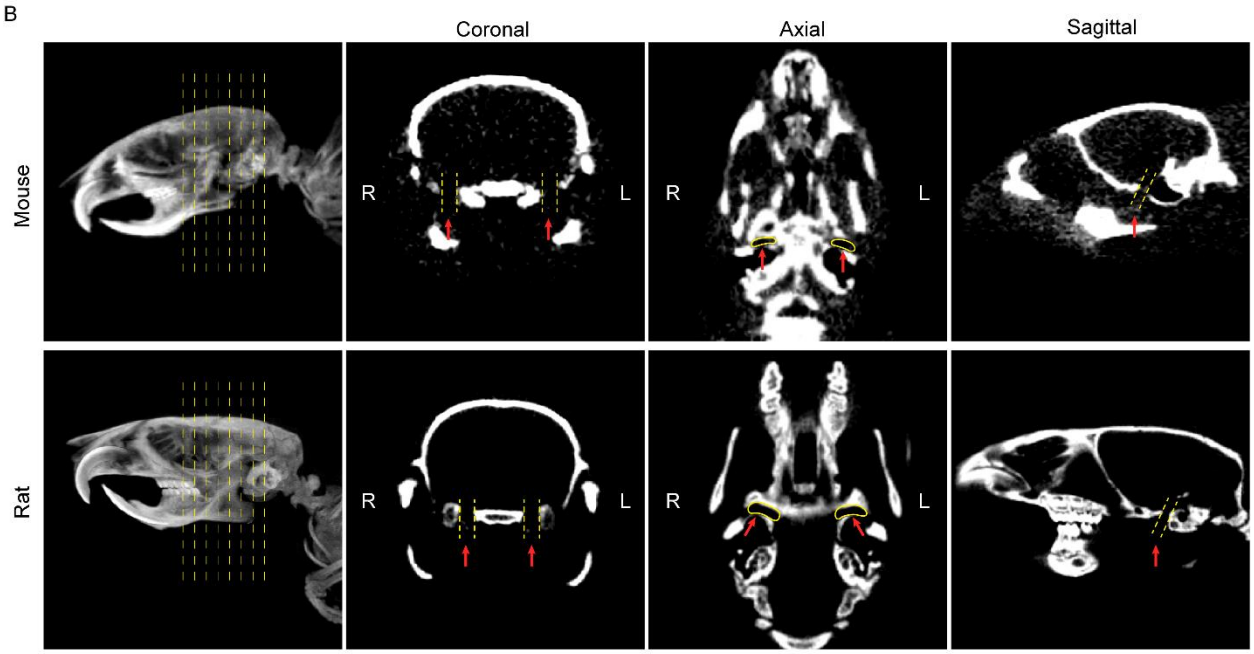

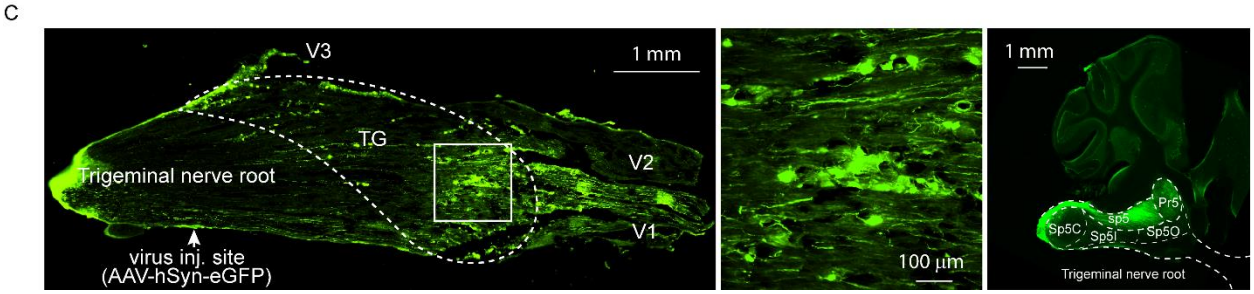

Figure 1: Foramen lacerum anatomy. A) The foramen lacerum in the skull base of human and rodents. Pictures of skull bases of human, SD rat, CD1 mouse, and C57BL/7 mouse were taken, schemes of trigeminal nerve system (yellow color) was overlayed in the skull base of rodents to depict the relationship between the foramen lacerum and trigeminal system. **B)** Computed tomography (CT) of the foramen lacerum. SD rats and C57BL/7 mouse were anesthetized and scanned with CT machine. Three-dimensional reconstruction was performed to obtain coronal, axial, and sagittal views highlighting the foramen lacerum (red arrow). **C)** Virus delivery through foramen lacerum. AAV1 was directly injected with pulled glass pipette to the trigeminal nerve root (n=3). The virally expressed GFP was captured and shown for the trigeminal system.

Figure 2

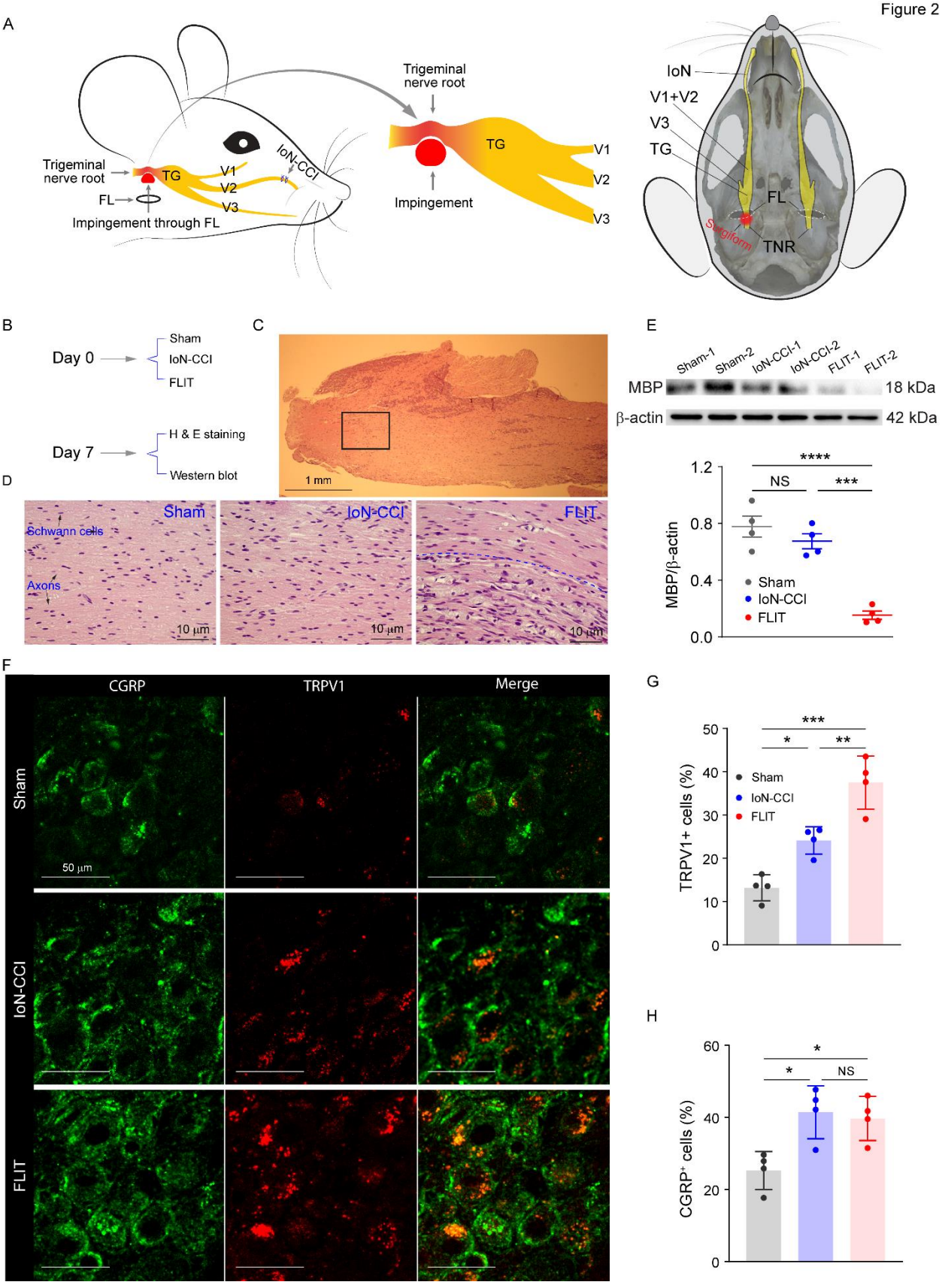
A
Trigeminal nerve root
TG
V1
V2
V3
FL
Impingement through FL
IoN-CCI
Trigeminal nerve root
TG
V1
V2
V3
Impingement
IoN
V1+V2
V3
TG
FL
Supraform
TNR
B
Day 0
Sham
IoN-CCI
FLIT
Day 7
H & E staining
Western blot
C
1 mm
D
Sham
IoN-CCI
FLIT
Schwann cells
Axons
10 μm
10 μm
10 μm
E
Sham-1
Sham-2
IoN-CCI-1
IoN-CCI-2
FLIT-1
FLIT-2
MBP
18 kDa
β-actin
42 kDa
MBP/β-actin
****
NS
***
Sham
IoN-CCI
FLIT
F
CGRP
TRPV1
Merge
Sham
IoN-CCI
FLIT
50 μm
G
TRPV1+ cells (%)
***
*
**
Sham
IoN-CCI
FLIT
H
CGRP+ cells (%)
*
*
NS

Figure 2. Foramen lacerum impingement of trigeminal nerve root (FLIT) leads to demyelination of the trigeminal nerve root. A) Diagram of the FLIT and IoN-CCI (infraorbital nerve chronic constriction injury) procedure (left panel), and diagram of trigeminal nerve root impingement in the skull base (right panel). **B-D**) H&E staining of the trigeminal nerve root (n=4 per group). **B)** Diagram of study timeline. **C)** H&E staining at lower magnification. Boxed area indicates a representative view of the trigeminal nerve root. **D)** Trigeminal nerve root staining. Representative pictures of each group were shown. Myelinated fibers and Schwann cells were indicated in the picture from the Sham group. In the picture from the FLIT group, above the dashed line shows normal nerve fibers, and below the dashed line shows demyelinated fibers with inflammatory cell infiltration. **E)** Western blot using an anti-myeline basic protein antibody. Representative blots were shown from 4 animals per group. Quantification plot shows individual values of each mouse, with mean ± SEM shown in scatter plot. One-way ANOVA test with post hoc Tukey test was conducted. NS: not significant; ***p<0.001, ****p<0.0001. **F-H)** CGRP and TRPV1 staining (n=4 animals per group). **F)** Representative staining from each group. **G)** Percentage of $TRPV1^+$ cells among all neurons. **H)** Percentage of $CGRP^+$ cells among all neurons. Shown bar charts represent mean ± SD with each dot representing each animal. One way ANOVA test with post hoc Tukey test was conducted. NS: not significant; *p<0.05, **p<0.01, ***p<0.001.

Figure 3

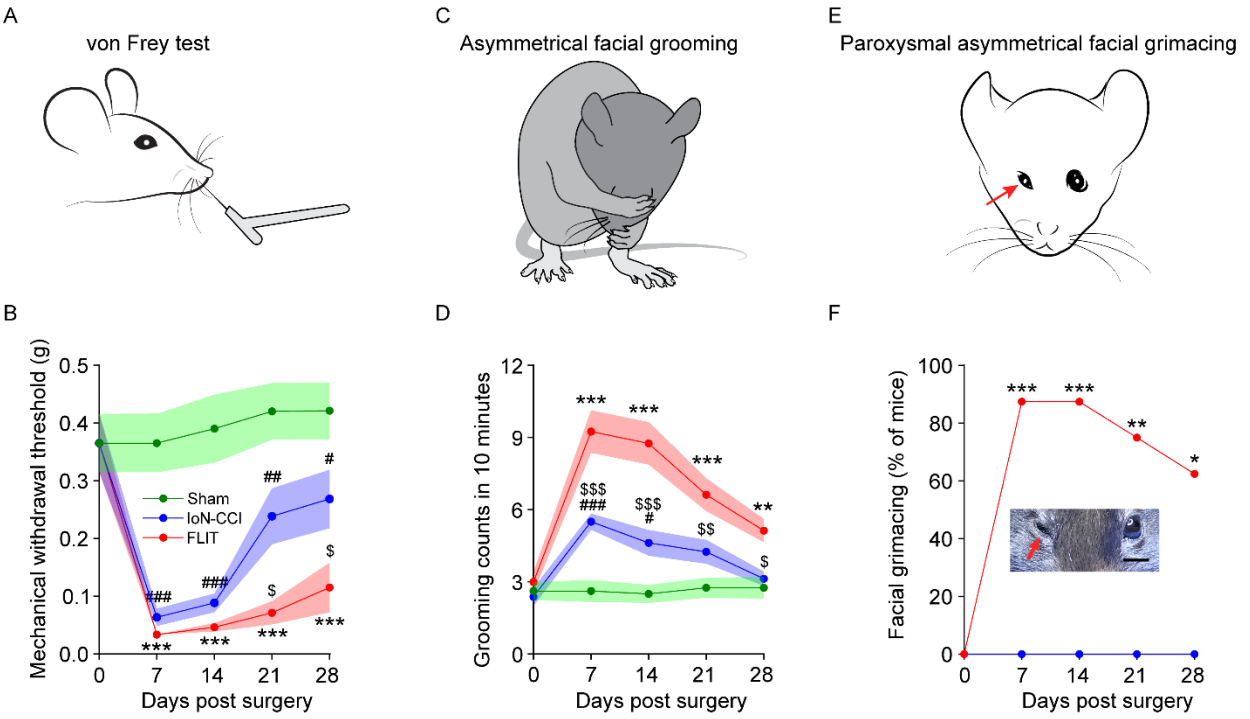

Figure 3. FLIT procedure leads to TN-like behavior. A-F) Mice underwent FLIT, IoN-CCI, and sham surgeries (n=8 per group, male), behavioral characteristics were assessed. Shown line charts represent mean ± SEM (in color shades), except for panel F. **A-B)** Facial mechanical withdrawal. There was a significant difference among the three groups using two-way ANOVA test. Post-hoc Bonferroni test revealed difference at indicated time points, FLIT vs. Sham, ***p<0.001; IoN-CCI vs. Sham, # p<0.05, ## p<0.01, ###p<0.001; FLIT vs. IoN-CCI, $ p<0.05. **C-D)** Asymmetrical facial grooming was prominent in the FLIT group. Grooming counts (including asymmetrical and symmetrical grooming) in ten minutes were recorded at indicated time points. There was a significant difference among the three groups using two-way ANOVA test. Post-hoc Bonferroni test revealed difference at indicated time points, FLIT vs. Sham, **p<0.01, ***p<0.001; IoN-CCI vs. Sham, # p<0.05, ###p<0.001; FLIT vs. IoN-CCI, $ p<0.05, $$ p<0.01, $$$ p<0.001. **E-F)** Paroxysmal asymmetrical facial grimacing. Percentages of mice with paroxysmal asymmetrical facial grimacing were recorded. Neither the IoN-CCI group nor the Sham group displayed this behavior, hence only data for the sham group were shown. Fisher's exact test was used for statistical analysis, *p<0.05, **p<0.01, ***p<0.001.

Figure 4

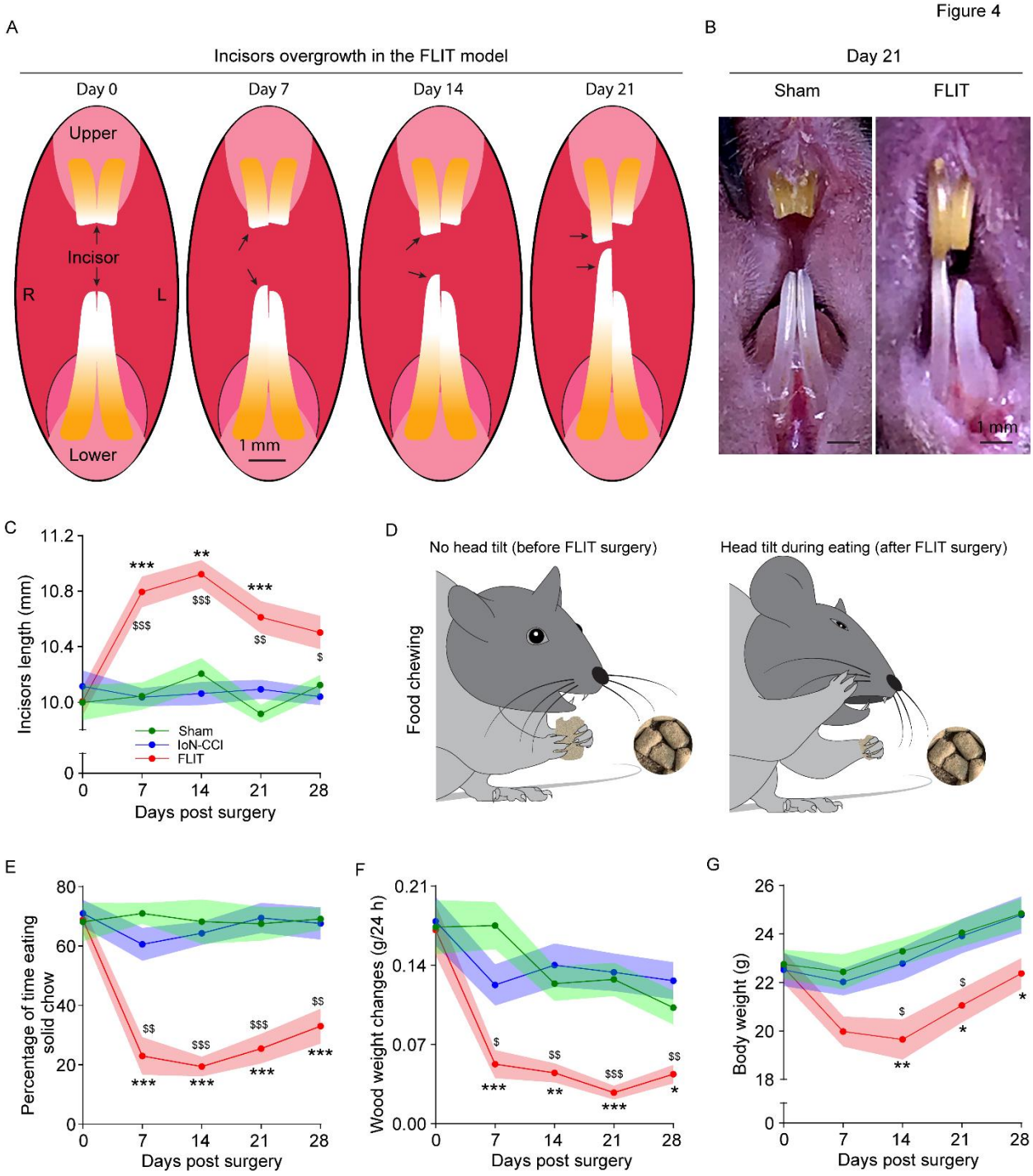

Figure 4. Dental pain-related behavior in the FLIT model. Mice underwent FLIT, IoN-CCI, and sham surgeries (n=8 per group, male). All line charts represent mean ± SEM (in color shades). **A)** Diagram of incisors overgrowth in the FLIT model. **B)** Representative picture of incisors overgrowth in the FLIT model. **C)** Incisors length. There was significant difference among the three groups using two-way ANOVA test. Post-hoc Bonferroni test revealed difference at indicated time points, FLIT vs. Sham,

p<0.01, ***p<0.001; FLIT vs. IoN-CCI, $ p<0.05, $$ p<0.01, $$$p<0.001. **D-E) Dental pain-like behaviors during food chewing. **D)** Diagram of head tilt during eating after the FLIT procedure. Left panel, no head tilt during food chewing prior to the FLIT surgery; right panel, head tilt while eating after FLIT surgery. **E)** Percentage of time eating solid chow was counted in 10 minutes. There was a significant difference among the three groups using two-way ANOVA test. Post-hoc Bonferroni test revealed difference at indicated time points, FLIT vs. Sham, ***p<0.001; FLIT vs. IoN-CCI, $$ p<0.01, $$$ p<0.001. **F)** Balsa wood weight changes. Mice were singly housed overnight with a balsa wood block and wood weight changes were quantified. There was a significant difference among the three groups using two-way ANOVA test. Post-hoc Bonferroni test revealed difference at indicated time points, FLIT vs. Sham, *p<0.05, **p<0.01, ***p<0.001; FLIT vs. IoN-CCI, $ p<0.05, $$ p<0.01, $$$p<0.001. **G)** Body weight changes after FLIT procedure. There weresignificant differences among the three groups using two-way ANOVA test. Post-hoc Bonferroni test revealed difference at indicated time points, FLIT vs. Sham, *p<0.05, **p<0.01; FLIT vs. IoN-CCI, $ p<0.05.

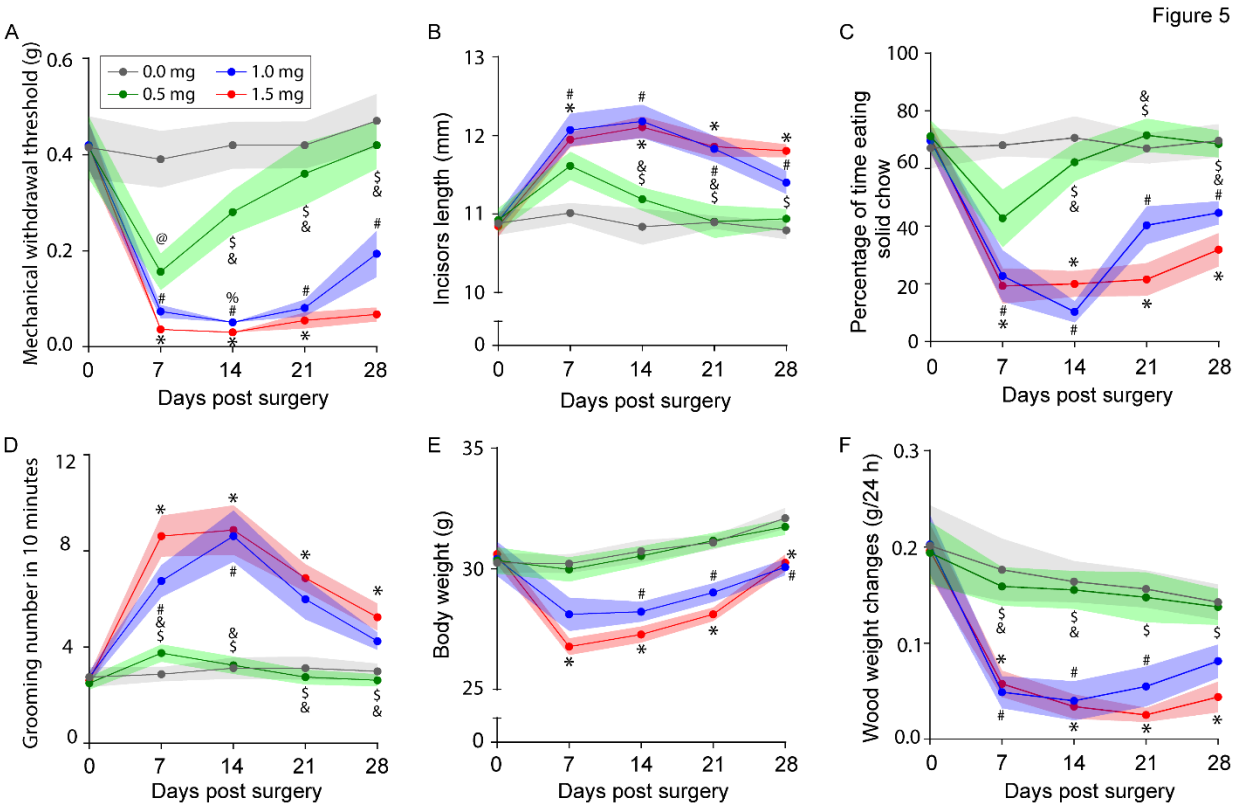

Figure 5. Doses of surgifoam and pain-like behavior. Mice (male) underwent FLIT procedure using different doses of surgifoam (0.0 mg-sham; 0.5 mg; 1.0 mg; and 1.5 mg), n=8 per group. Behavioral testing was performed at indicated time points. Shown line charts represent mean ± SEM (in color shades). **A**) Mechanical withdrawal threshold. **B**) Incisors length. **C**) Percentage of time chewing solid chew. **D**) Grooming counts in 10 minutes. **E**) Body weight changes. **F**) Wood weight changes in 24 hours. There was significant difference among the four groups using two-way ANOVA test. Post-hoc Bonferroni test revealed difference at indicated time points, all symbols represented $p<0.05$. Specific comparisons were '*' 0 mg vs. 1.5 mg; '$' 0.5 mg vs. 1.5 mg; '@' 0 mg vs. 0.5 mg; '%' 1.0 mg vs. 1.5 mg; '#' 0 mg vs. 1.0 mg; and '&' 0.5 mg vs. 1.0 mg.

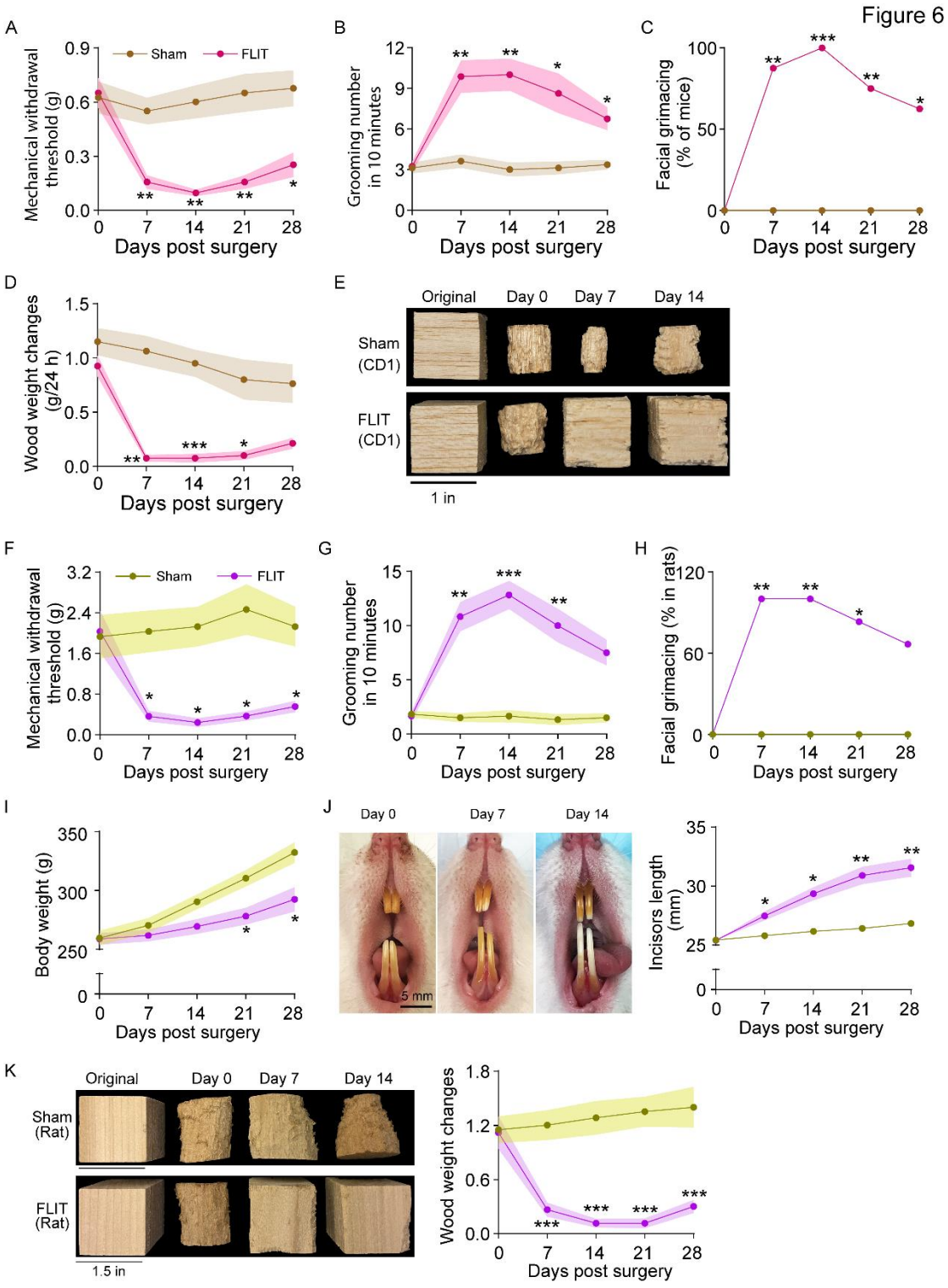

Figure 6. FLIT model in CD1 mice and SD rats. A-E) FLIT model in CD1 mice. CD1 mice underwent FLIT or sham procedure (n=8 per group, male) and were assessed for behavior: **A**) facial mechanical withdrawal threshold; **B)** grooming counts in 10 minutes; **C)** percentage of mice with facial grimacing; **D)**

balsa wood weight changes; **E)** representative pictures of balsa wood blocks in sham and FLIT groups. **F-K)** FLIT model in male SD rats. SD rats underwent FLIT or sham procedure (n=6 per group) and were assessed for behavior: **F)** facial mechanical withdrawal threshold; **G)** grooming counts in 10 minutes; **H)** percentage of mice with facial grimacing; **I)** body weight; **J)** left panel, representative images of incisors in rats underwent FLIT. right panel, incisors length; **K**) left panel, representative pictures of pine wood blocks in sham and FLIT groups. right panel, wood block weight changes. Shown line charts represents mean ± SEM (in color shades) except for panel C and H). Two-way ANOVA test was used for panels A, B, D, F, G, I, J and K and there was statistically significant difference present between the group. Post-hoc Bonferroni test was used to determine the time points at which the difference existed. FLIT vs. sham: *p<0.05; **p<0.01, ***p<0.001. Fisher's exact test was used for panel C and H, *p<0.05, **p<0.01, ***p<0.001.

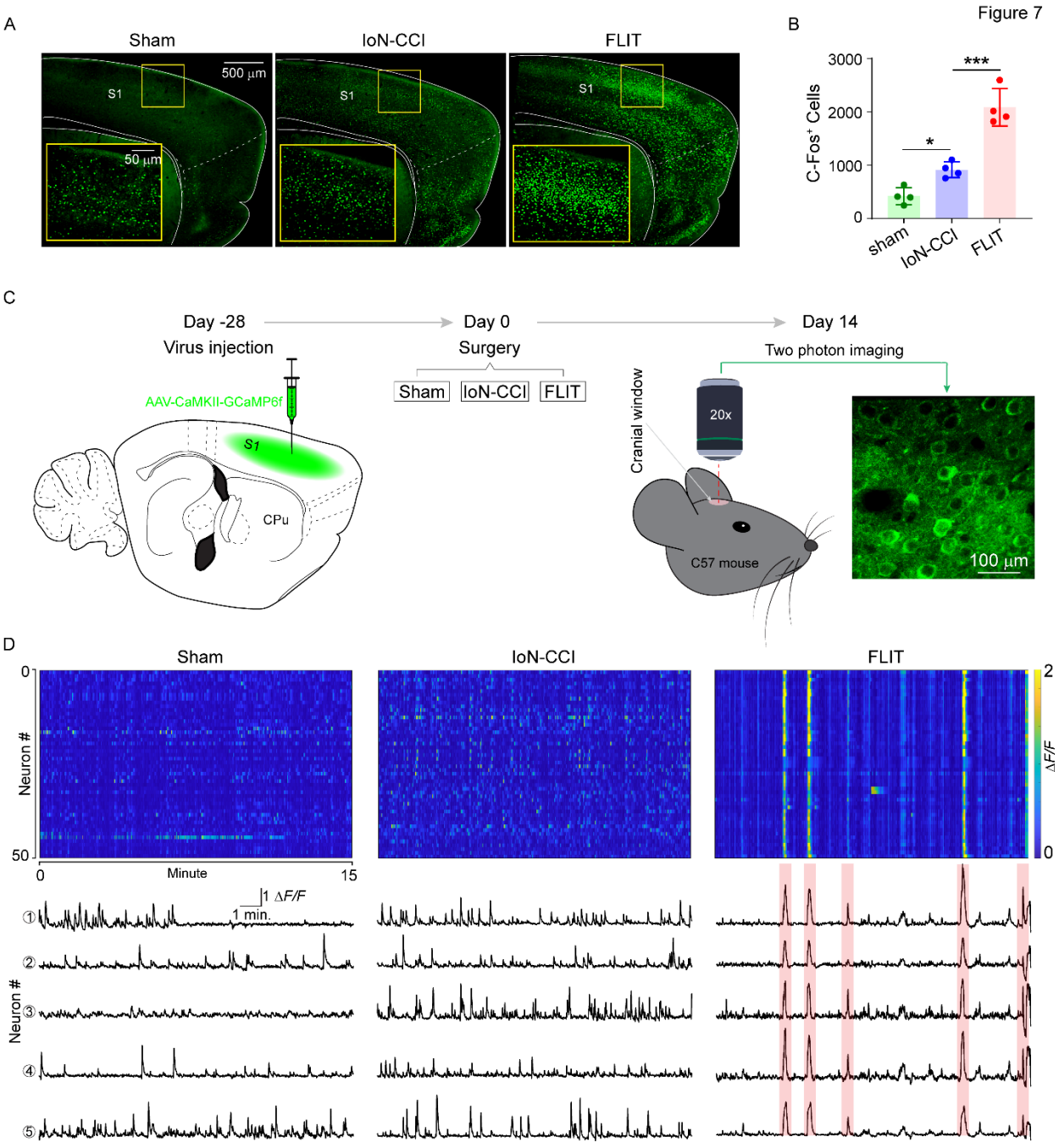

Figure 7. Unique cortical neural activation pattern in the FLIT model. A-B) c-Fos+ cells in the FLIT model. Mice (n=4 per group) underwent FLIT, IoN-CCI, and sham surgeries. Two hours after surgery, brains were obtained for c-Fos staining. **A)** Representative c-Fos staining in different groups. **B)** Number of c-Fos positive cells in the S1 cortex. One-way ANOVA indicated statistically significant difference was present among groups. Post-hoc Tukey test was performed. *P<0.05, ***p<0.001. **C-D)** Two-photon calcium imaging in awake and resting state. Mice (n=4 per group) underwent S1 cortex microinjection of AAV8-CaMKII-GCaMP6f and were allowed 4 weeks for virus expression. Two-photon calcium imaging

was performed without anesthesia at a resting state. **C)** Experimental design. Left sketch depicts virus injection in S1 of mouse followed by surgeries at day 0. The panel on the far-right was a representative image taken during two-photon imaging session to demonstrate GCaMP6f expression. **D)** Top panels were heatmaps of calcium dynamics. For all heatmaps, 50 neurons were shown over 15 minutes of imaging time. Color represented $\Delta F/F$: blue color - lower values of $\Delta F/F$, yellow color - higher values of $\Delta F/F$. Lower panels showed representative calcium tracing from the imaging field. Five representative single neurons were shown. Red color marked synchronized firing.